Mon. Not. R. Astron. Soc. **341,** 509–516 (2003)

Interaction between the north-eastern boundary of Sgr A East and giant molecular clouds

Sungho Lee,[1,2] Soojong Pak,[1,2★] Christopher J. Davis,[3] Robeson M. Herrnstein,[4] T. R. Geballe,[5] Paul T. P. Ho[4] and J. Craig Wheeler[6]

[1] *Astronomy Programme in SEES, Seoul National University, Shillim-Dong, Kwanak-Gu, Seoul 151-742, South Korea*
[2] *Korea Astronomy Observatory, Whaam-Dong, Youseong-Gu, Taejeon 305-348, South Korea*
[3] *Joint Astronomy Centre, University Park, 660 North A'ohökü Place, Hilo, HI 96720, USA*
[4] *Harvard–Smithsonian Center for Astrophysics, 60 Garden Street, Cambridge, MA 02138, USA*
[5] *Gemini Observatory, 670 N. A'ohökü Place, Hilo, HI 96720, USA*
[6] *Astronomy Department, University of Texas, Austin, TX 78712, USA*

Accepted 2003 January 13. Received 2002 November 29; in original form 2002 September 23

ABSTRACT

We have detected the $v = 1 \rightarrow 0$ S(1) ($\lambda = 2.1218$ μm) and $v = 2 \rightarrow 1$ S(1) ($\lambda = 2.2477$ μm) lines of H_2 in the Galactic Centre, in a 90×27 arcsec^2 region between the north-eastern boundary of the non-thermal source Sgr A East, and the giant molecular cloud (GMC) M−0.02 − 0.07. The detected H_2 $v = 1 \rightarrow 0$ S(1) emission has an intensity of 1.6–21 $\times 10^{-18}$ W m^{-2} arcsec^{-2} and is present over most of the region. Along with the high intensity, the large linewidths (FWHM = 40–70 km s^{-1}) and the H_2 $v = 2 \rightarrow 1$ S(1) to $v = 1 \rightarrow 0$ S(1) line ratios (0.3–0.5) can be best explained by a combination of C-type shocks and fluorescence. The detection of shocked H_2 is clear evidence that Sgr A East is driving material into the surrounding adjacent cool molecular gas. The H_2 emission lines have two velocity components at ∼+50 and ∼0 km s^{-1}, which are also present in the NH_3(3, 3) emission mapped by McGary, Coil & Ho. This two-velocity structure can be explained if Sgr A East is driving C-type shocks into both the GMC M−0.02 − 0.07 and the northern ridge of McGary et al.

Key words: ISM: individual: Sgr A East – ISM: individual: M−0.02 − 0.07 – ISM: lines and bands – ISM: molecules – Galaxy: centre – infrared: ISM.

1 INTRODUCTION

Sgr A East has frequently been interpreted as a supernova remnant because of its shell structure and non-thermal spectrum (Jones 1974; Goss et al. 1983 and references therein; and see the more recent references in Maeda et al. 2002). Some recent research, however, has suggested that the energetics, size, and elongated morphology (3×4 arcmin^2 or 7×9 pc^2 at $d = 8.5$ kpc) of Sgr A East cannot have been produced by a typical supernova (Yusef-Zadeh & Morris 1987; Mezger et al. 1989). Mezger et al. (1989) estimate the required energy to produce Sgr A East to be more than 4×10^{52} erg. Modelling of the entire spectrum of Sgr A East by Fatuzzo et al. (1999), which fits very well with the observations of the non-thermal emission of Sgr A East and EGRET γ-ray sources, supports the energy estimate by Mezger et al. (1989). Those authors concluded that a single supernova explosion could explain the existence of Sgr A East only if it occurred within the cavity formed by the stellar wind from a progenitor star. In that scenario, however, the formation of the cavity takes too much time (∼10^6 yr) compared with the orbital period (∼10^5 yr) of matter circling around the Galactic Centre (Mezger et al. 1989).

Yusef-Zadeh & Morris (1987) suggested that a different kind of explosive event could create Sgr A East. The energy required to make a huge shell such as Sgr A East has been associated with a 'hypernova' (Woosley, Eastman & Schmidt 1999). Khokhlov & Melia (1996) hypothesize that Sgr A East may be the remnant of a solar-mass star tidally disrupted by a massive black hole. Their model can naturally explain the elongated shape of Sgr A East as well as the extreme energetics. However, from their observation with the *Chandra X-ray Observatory*, Maeda et al. (2002) suggest that Sgr A East should be classified as a metal-rich 'mixed morphology' supernova remnant. They argue that the model of Khokhlov & Melia (1996) cannot reproduce the metal-rich abundances observed at the centre of Sgr A East. They also conclude that a single Type II supernova explosion with an energy of 10^{51} erg into a homogeneous ambient medium with a density of 10^3 cm^{-3} can most simply explain the results of both radio and X-ray observations, and thus that the extreme energy of ∼10^{52} erg is not required.

In principle, the energy of the explosive event can be directly measured by studying regions where Sgr A East is colliding with

★E-mail: soojong@kao.re.kr

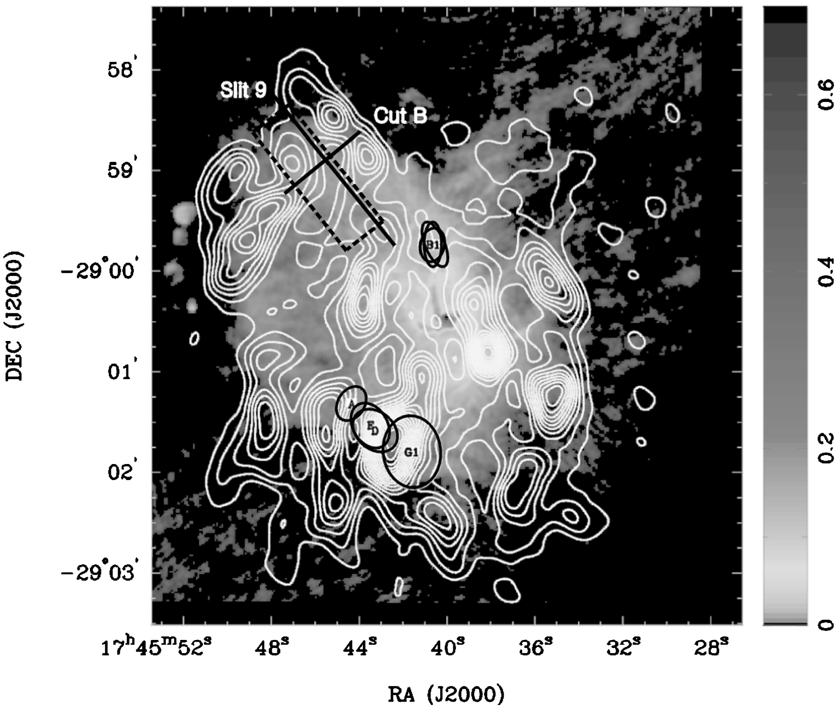

Figure 1. Central 10×15 pc^2 region of the Galaxy. Contours representing the velocity-integrated map of $NH_3(3, 3)$ emission are overlaid on a 6-cm continuum image of the Sgr A complex from fig. 10 of McGary et al. (2001). The black dot at the centre of the image is Sgr A* and the mini-spiral is Sgr A West. The CND is traced by the brighter part of the continuum surrounding them, and Sgr A East is seen as the outer part extending to the boundary of the NH_3 contours. The GMC M−0.02 − 0.07 lies to the east of this region. The dashed box at the north-eastern edge of Sgr A East encloses the 90×27 arcsec^2 region observed in H_2. The two solid lines in the box are the locations from which the H_2 spectra shown in this paper were extracted. Cut B is made across the 10 slits, while the north-east–south-west cut, perpendicular to the edge of Sgr A East, is slit 9. Letters mark the positions of OH(1720 MHz) masers with error ellipses scaled up by a factor of 15 (Yusef-Zadeh et al. 1999a).

ambient interstellar material. By tracing the dynamics of molecular gas, an interaction between the eastern part of Sgr A East and the giant molecular cloud (GMC) M−0.02 − 0.07 (also known as the '50 km s^{-1} cloud') has been inferred (Genzel et al. 1990; Ho et al. 1991; Serabyn, Lacy & Achtermann 1992; Mezger, Duschl & Zylka 1996; Novak 1999; Coil & Ho 2000). Recent observations of $NH_3(3, 3)$ emission in the region show that Sgr A East impacts material to the north and west as well (see Fig. 1) (McGary, Coil & Ho 2001). As direct evidence of this interaction, several 1720-MHz OH masers, which are a good diagnostic of the continuous, or C-type, shock excitation (Frail et al. 1996; Wardle, Yusef-Zadeh & Geballe 1999), have been detected along the southern edge of Sgr A East and to the north of the circumnuclear disc (CND) (Yusef-Zadeh et al. 1996).

Wardle et al. (1999) and Yusef-Zadeh et al. (1999b, 2001) detected H_2 line emission in regions where OH masers have been detected. In most cases H_2 line emission arises either from thermal excitation (e.g. by shock heating) or from non-thermal excitation by far-ultraviolet absorption (Black & van Dishoeck 1987; Burton 1992; Pak et al. 1998). One can in principle distinguish between these two mechanisms by comparing near-infrared (near-IR) line intensities. The H_2 $v = 2 \rightarrow 1$ S(1)/$v = 1 \rightarrow 0$ S(1) ratio has been an effective discriminant in a number of shocked regions (where the ratio should be $\leqslant 0.3$) and photodissociation regions (PDRs) (where it is about 0.5–0.6). However, a 'thermal' line ratio can be observed in a PDR – even though fluorescence is the dominant excitation mechanism – if the gas density is high ($\geqslant 10^5$ cm^{-3}: Sternberg & Dalgarno 1989). Gatley et al. (1984) observed the CND and concluded that the H_2 molecules are excited by collisions, while the results for larger regions (about $2^\circ \times 2^\circ$) by Pak, Jaffe & Keller (1996a,b) are consistent with non-thermal excitation. The interpretation of Wardle et al. (1999) and Yusef-Zadeh et al. (1999b, 2001) that the line emission in Sgr A East is thermal is supported by the presence of the 1720-MHz OH masers. It is therefore likely that Sgr A East is indeed driving shocks into the adjacent GMCs to the south and into the CND.

The fields observed by Wardle et al. (1999) and Yusef-Zadeh et al. (1999b, 2001) are restricted to the vicinity of the CND and cover only some of the regions where interaction of the Sgr A East shell with surrounding material is expected. Before one can hope to estimate the energy released in the event that created Sgr A East, it is necessary to observe additional interaction regions in diagnostic lines of H_2 at high spectral resolution. In this paper we present velocity-resolved, near-IR H_2 observations at the north-eastern boundary of Sgr A East. By measuring H_2 $v = 2 \rightarrow 1$ S(1)/$v = 1 \rightarrow 0$ S(1) line ratios and line profiles simultaneously, we aim to study the excitation and kinematics of the interaction between Sgr A East and M−0.02 − 0.07.

2 OBSERVATION AND DATA REDUCTION

We observed the H_2 $v = 1 \rightarrow 0$ S(1) ($\lambda = 2.1218$ μm) and the H_2 $v = 2 \rightarrow 1$ S(1) ($\lambda = 2.2477$ μm) spectra at the 3.8-m United Kingdom Infra-Red Telescope (UKIRT) in Hawaii on 2001 August 3 and 4 (UT), using the Cooled Grating Spectrometer 4 (CGS4; Mountain et al. 1990) with a 31 line mm^{-1} echelle grating, 300-mm focal length camera optics and a two-pixel-wide slit. The spatial resolution along the slit was 0.90 arcsec for H_2 $v = 1 \rightarrow 0$ S(1) with a grating angle of 64°.691 and 0.84 arcsec for H_2 $v = 2 \rightarrow 1$ S(1) with a grating angle of 62°.127; the slit widths on the sky were 0.83 and 0.89 arcsec, respectively, for these two configurations. The slit length was ~90 arcsec. The instrumental resolutions, measured from Gaussian fits to sky lines in our raw data, were ~17 km s^{-1} for H_2 $v = 1 \rightarrow 0$ S(1) and ~19 km s^{-1} for H_2 $v = 2 \rightarrow 1$ S(1).

10 parallel slit positions were observed, sampling a 90 × 27 arcsec^2 area on the north-eastern boundary of Sgr A East. The slit was oriented 40° east of north for each measurement; adjacent slit positions were separated by 3 arcsec perpendicular to the slit axis. The coordinates at the centre of the observed area are $\alpha = 17^h45^m45^s.9$, $\delta = -28°59'05''$ (J2000) (see Fig. 1). The south-western part of this region includes the 'outer H_2 clumps' from which H_2 emission was detected by Yusef-Zadeh et al. (2001). Only the ninth slit position, hereafter called 'slit 9', was observed in both H_2 $v = 1 \rightarrow 0$ S(1) and H_2 $v = 2 \rightarrow 1$ S(1). The telescope was nodded between object and blank-sky positions every 25 min, to subtract the background and telluric OH line emission. The sky positions were offset by about 2°.5 ($\Delta\alpha = -2°.03$, $\Delta\delta = 0°.85$) from the on-source positions.

Initial data reduction steps, involving bias-subtraction and flat-fielding (using an internal blackbody lamp), were accomplished by the automated Observatory Reduction and Acquisition Control (ORAC) pipeline at UKIRT. IRAF was used for the remainder of the reduction. We corrected the spectral distortion along the dispersion axis using the spectrum of the standard star HR 6496 as a template. The sky OH lines were then used to correct for spatial distortion perpendicular to this axis and also for wavelength calibration. We also corrected for the motions of the Earth and Sun in order to determine local standard of rest (LSR) velocities.

Only part of the flux from a standard star is detected because of the narrow slit; hence for proper flux calibration the measured signal must be corrected. We assumed a circularly symmetric point spread function (PSF) for the star, based on the flux profile along the slit length, to estimate the missing flux. The correction factor, which varies with the seeing, ranged from 2.06 to 2.56. Near-IR emission from the Galactic Centre is attenuated by interstellar material in the foreground (mostly 4–8 kpc from the Galactic Centre) and by material in the Galactic Centre itself. Since we believe that the H_2 line emission originates from the surface of the cloud, we ignore the latter (Pak et al. 1996a,b) and correct only for foreground extinction, which we assume to be $A_K = 2.5$ mag (Catchpole, Whitelock & Glass 1990).

3 RESULTS AND DISCUSSION

3.1 H_2 $v = 1 \rightarrow 0$ S(1) emission

Bright (1.6–21 × 10^{-18} W m^{-2} arcsec^{-2}) H_2 emission was detected from most of the observed region (90 × 27 arcsec^2) along the north-eastern boundary of Sgr A East. We created a south-east–north-west cut parallel to the boundary of Sgr A East ('cut B') by extracting spectra from each of the 10 slit positions. A second cut perpendicular to the boundary (i.e. south-west–north-east) is composed of six positions from slit 9. The positions of cut B and slit 9 are marked in Fig. 1. Along cut B, the intensity of NH_3 emission varies dramatically; we can investigate both high- and low-density regions along this cut. Slit 9 is the only slit observed in both H_2 $v = 1 \rightarrow 0$ S(1) and $v = 2 \rightarrow 1$ S(1), the line ratio of which we can use to constrain models for the excitation of H_2. In this paper, we present the results of these two cuts, rather than the whole data set, as a preliminary report. We aim to concentrate on the excitation mechanism of the detected H_2 emission, and to map the structure and kinematics perpendicular to and parallel to the boundary. From the 16 H_2 $v = 1 \rightarrow 0$ S(1) spectra in Figs 2 and 3 we measure line centres and linewidths along the interaction region. Each spectrum is well fitted by one or two Gaussian components.

Figs 4 and 5 show the distributions of the derived H_2 $v = 1 \rightarrow 0$ S(1) line parameters along cut B and slit 9, respectively. For direct comparison, we include in these figures data from the NH_3(3, 3) observations of McGary et al. (2001); the NH_3 emission essentially traces the cool ($\lesssim$100 K), dense (10^5 cm^{-3}) cloud material. From these data we note the following.

(i) In Figs 4(a) and 5(a) there are two velocity components, at $V_{LSR} \sim 0$ and ~+50 km s^{-1}. Both components are evident in H_2 and NH_3, although the 0 km s^{-1} features are not spatially coincident. The variation in the velocity of either component is less than ~20 km s^{-1} along both slit 9 and cut B.

(ii) The H_2 linewidths in Figs 4(b) and 5(b) are much larger than the NH_3 widths and show no obvious trend along either slit 9 or cut B.

(iii) Along cut B, the distribution of the total intensity of H_2 (the solid line in Fig. 4c) is quite different from that of NH_3 (the dashed line). The NH_3 emission increases to the south-east as the cut passes deeper into the body of the GMC M−0.02 − 0.07, but the H_2 emission decreases in this direction. The decrease in H_2 may be explained by exhaustion of the source of excitation (e.g. shock energy or ultraviolet photons) or by obscuration, at the inner, more dense regions of the cloud, or by the geometry of the interaction region (see Section 3.3).

(iv) Along slit 9, the distribution of the H_2 intensity (solid line) in Fig. 5(c) is generally similar to that of NH_3 (dashed line). It should be noted that NH_3 is attenuated at positions greater than +30 arcsec by the edge of the primary beam in the Very Large Array (VLA) mosaic (McGary et al. 2001). There is a small discrepancy between NH_3 and H_2 between +10 and +30 arcsec which may be the result of the same effects discussed for cut B. Note that slit 9 covers a very large spatial scale (90 arcsec). The brightest emission along slit 9, between offsets −20 and −45 arcsec (the south-western part), arises from the outer H_2 clumps of Yusef-Zadeh et al. (2001).

3.2 H_2 excitation

The H_2 $v = 2 \rightarrow 1$ S(1) line was detected at three locations along slit 9, at positions 23.7 arcsec north-east, 10.5 arcsec south-west and 22.2 arcsec south-west relative to the centre of the slit ($\alpha = 17^h45^m45^s.3$, $\delta = -28°58'58''$; J2000). From these data we measured line ratios [H_2 $v = 2 \rightarrow 1$ S(1)/$v = 1 \rightarrow 0$ S(1)] of 0.40 ± 0.12, 0.51 ± 0.17 and 0.27 ± 0.07, respectively (see Fig. 3). At other positions only the H_2 $v = 1 \rightarrow 0$ S(1) line was detected, with 3σ upper limits to the ratio of 0.5, 0.6 and 0.1 at offsets of 31.8 arcsec north-east, 4.8 arcsec north-east and 44.7 arcsec south-west along slit 9, respectively.

Fluorescent excitation in a low-density PDR [$n(H_2) < 5 \times 10^4$ cm^{-3}] should yield a ratio of about 0.6. A lower ratio is expected in a more dense PDR environment (Black & van Dishoeck 1987), or in a shock. There are two basic types of shock: 'jump' or J-type and 'continuous' or C-type (see Draine & McKee 1993 for a review). A J-type shock is formed in a highly ionized or weakly magnetized gas. Fluid parameters such as density and temperature undergo a discontinuous change (jump) at the shock front where the molecules may be dissociated. J-type shocks (with velocities greater

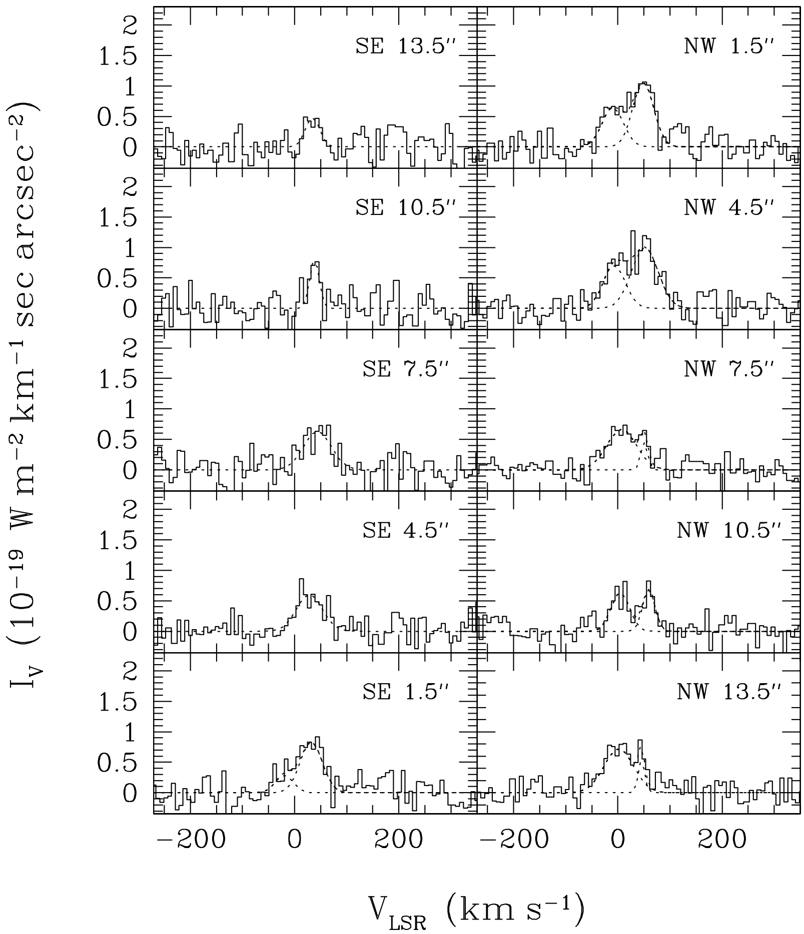

Figure 2. H_2 $v = 1 \rightarrow 0$ S(1) spectra at 10 positions along cut B. Indicated positions are relative to the centre of the cut ($\alpha = 17^h45^m46\overset{s}{.}1$, $\delta = -28°59'01''$; J2000). The dotted lines are Gaussian fits to the observed line profiles. The spectra are not corrected for instrumental broadening.

than about 24 km s^{-1}) will completely dissociate the molecules (Kwan 1977); H_2 emission occurs from a warm, recombination plateau in the post-shock region. J-type shocks typically produce low line intensities and H_2 $v = 2 \rightarrow 1$ S(1)/$v = 1 \rightarrow 0$ S(1) line ratios as large as 0.5 are possible (Hollenbach & McKee 1989). At lower shock velocities, below the H_2 dissociation speed limit, J-type shocks may yield much lower line ratios: <0.3 (Smith 1995). In a C-type shock, where the magnetic field softens the shock front via ion–magnetosonic wave propagation so that the fluid parameters change continuously across the shock front, the H_2 dissociation speed limit is much higher (∼45 km s^{-1}, depending on the density and magnetic field strength in the pre-shock gas). Smaller line ratios of about 0.2 are then predicted (Smith 1995; Kaufman & Neufeld 1996).

From the observed ratios alone we are not able to distinguish unambiguously between excitation mechanisms. Our results can be explained by fast J-type shocks or dense PDRs, or by a combination of fluorescence and either C-type shocks or slow J-type shocks, since the higher line ratios associated with fluorescence will be tempered by the low H_2 $v = 2 \rightarrow 1$ S(1) intensities associated with collisional excitation in shocks.

To help to distinguish between the H_2 excitation mechanisms, we consider kinematic information and the spatial variation of the line ratio along slit 9. At most positions in Figs 4(b) and 5(b), the H_2 linewidths are high (typically 40–70 km s^{-1}, but as high as 120 km s^{-1} in some positions). This suggests shock excitation and turbulent motions in the gas and tends to exclude the pure fluorescence models (in which the H_2 line emission generally arises from the stationary gas at the edges of neutral clouds illuminated by far-ultraviolet photons from early-type stars). However, in other shocked regions the line ratio is found to be constant over a wide range of H_2 $v = 1 \rightarrow 0$ S(1) intensities and spatial positions (Davis & Smith 1995; Richter, Graham & Wright 1995), although this is not necessarily predicted from theory (Draine & McKee 1993). Conversely, in a PDR the ratio is sensitive to the incident far-ultraviolet flux and the molecular gas density [the H_2 $v = 1 \rightarrow 0$ S(1) intensity increases but the H_2 $v = 2 \rightarrow 1$ S(1)/$v = 1 \rightarrow 0$ S(1) ratio decreases with increasing gas density or ultraviolet intensity: Usuda et al. 1996; Takami et al. 2000]. Thus an unchanging H_2 $v = 2 \rightarrow 1$ S(1)/$v = 1 \rightarrow 0$ S(1) ratio is found in shocks, while a varying ratio is expected in the pure fluorescent case. The measured line ratio and the H_2 $v = 1 \rightarrow 0$ S(1) intensity in Fig. 5(c) show evidence of an anti-correlation in our data, as expected in dense PDRs. Although the wide line profiles point to shock excitation, fluorescence appears to play a significant role at at least some locations.

Considering the kinematics further, we note that J-type shocks produce narrow lines which peak at the velocity of the shock, while C-type shocks produce broader lines which peak at the velocity of the pre-shock gas and extend up to the shock velocity. Figs 4(a) and 5(a) show that there are two velocity components that are similar in

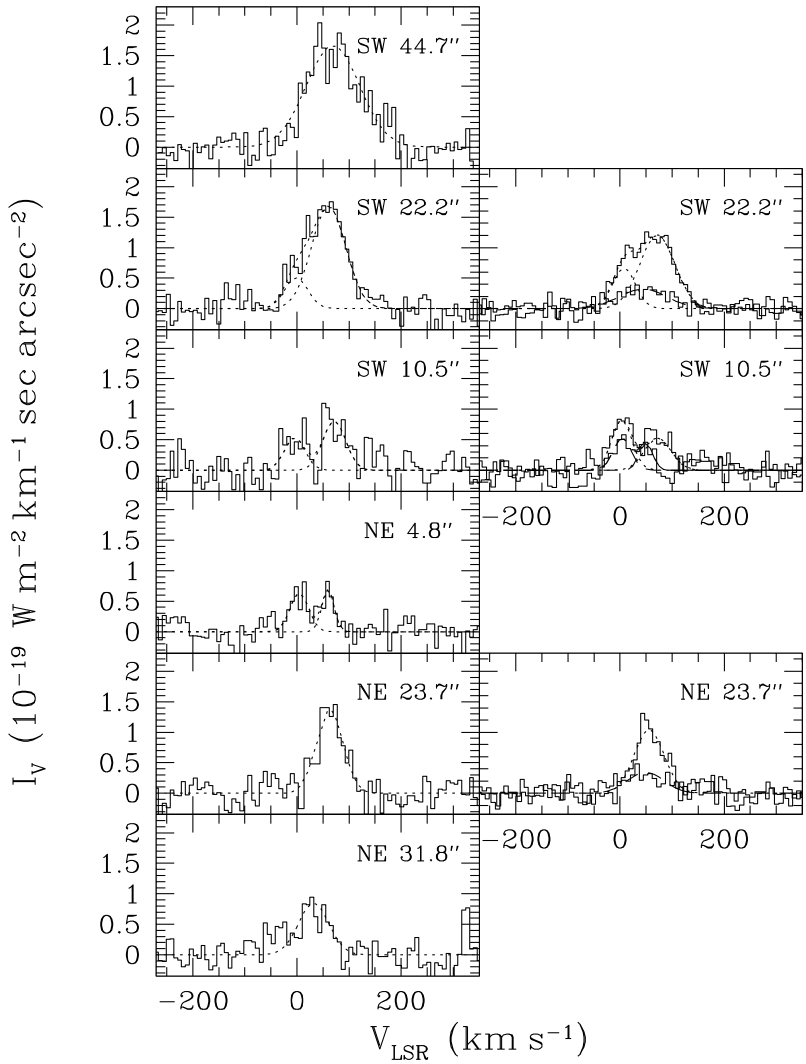

Figure 3. H_2 $v=1\rightarrow0$ S(1) and H_2 $v=2\rightarrow1$ S(1) spectra from six positions along slit 9. Indicated positions are relative to $\alpha = 17^h45^m45\overset{s}{.}3$, $\delta = -28°58'58''$ (J2000). The left-hand panels show the H_2 $v=1\rightarrow0$ S(1) spectra. The three right-hand panels present both the H_2 $v=1\rightarrow0$ S(1) and H_2 $v=2\rightarrow1$ S(1) spectra from the positions where H_2 $v=2\rightarrow1$ S(1) emission is detected; these are averaged over 3.4 arcsec on the sky to improve the signal-to-noise ratios. The other aspects are the same as for Fig. 2.

H_2 and NH_3. The H_2 emission traces hot (∼2000 K) gas and the NH_3 cool ($\lesssim$100 K) gas. Thus, if we assume that shocks are driven by Sgr A East into cold molecular gas with velocities given by the NH_3 data, then fast J-type shocks are inconsistent with our results, owing to the low peak velocities of the H_2 lines relative to the molecular clouds.

In summary, then, the wide line profiles and low peak velocities indicate C-type shock excitation. However, the high values of the line ratio at some positions along slit 9 and the spatial variation in that ratio point to a fluorescent component to the excitation in some locations. A combination of C-type shocks and fluorescence (see e.g. Fernandes, Brand & Burton 1997) is therefore the most reasonable explanation for the H_2 excitation. For the fluorescence, the source of the ultraviolet radiation could be either nearby early-type stars or J-type shocks. However, as noted above, we see no evidence of J-type shocks in our data. Also, we cannot establish whether nearby stars are the source of the ultraviolet flux owing to the lack of information on where or how many early-type stars there are in the region.

3.3 Structure of the interaction region

The extended +50 km s^{-1} component of the NH_3 emission traces the GMC M−0.02 − 0.07, while the 0 km s^{-1} component corresponds to the ‘northern ridge’ of McGary et al. (2001) [see the NH_3(3, 3) channel maps in their fig. 4]. The NH_3 component at ∼+20 km s^{-1} seen in Fig. 5(a) at negative offsets seems to trace hotter gas according to the NH_3(2, 2) to (1, 1) line ratio map by McGary et al. (2001), which they suggest may be the result of an impact by Sgr A East.

The difference in linewidth between NH_3 and H_2 as well as the different spatial locations of their 0 km s^{-1} features (Fig. 5a) indicate that the NH_3 and H_2 trace fundamentally different components of the gas. The small NH_3 linewidths arise in ambient clouds. The broader H_2 line emission traces shocked gas where the NH_3 molecules are probably destroyed. One can envision a situation in which Sgr A East is located adjacent to both M−0.02 − 0.07 (the +50 km s^{-1} component) and the northern ridge (the 0 km s^{-1} component), with Sgr A East driving C-type shocks into these clouds.

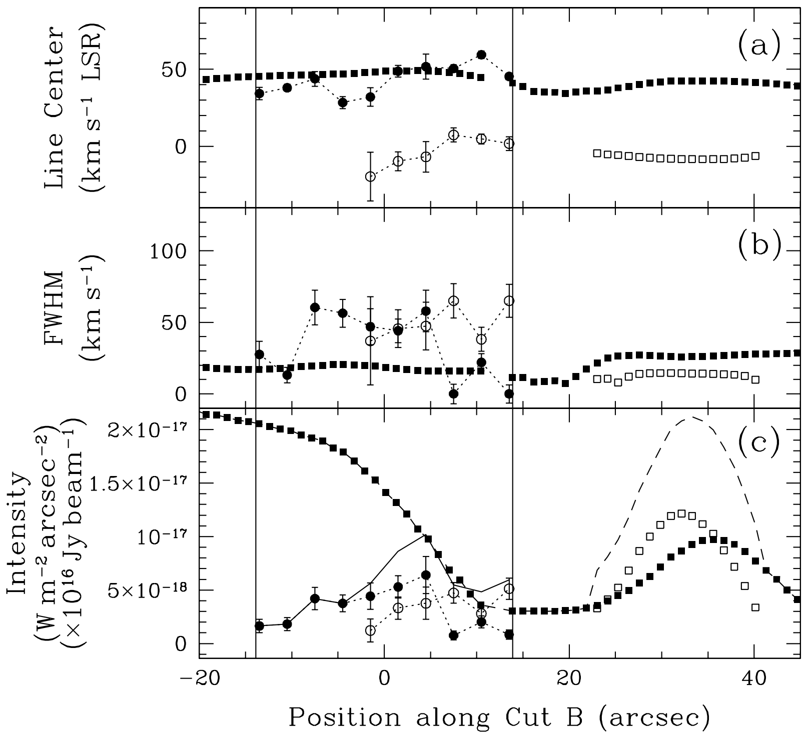

Figure 4. Derived line parameters for the spectra along cut B: (a) line centre velocity; (b) linewidth; and (c) integrated line intensity. Indicated positions are as in Fig. 2; positive towards the north-west. The filled circles and the open circles represent the +50 km s^{-1} component and the 0 km s^{-1} component of the H_2 $v = 1 \rightarrow 0$ S(1) spectra, respectively, and the filled and open squares the +50 and 0 km s^{-1} components of the NH_3(3, 3), from McGary et al. (2001). In panel (c), the solid and dashed lines denote the total intensity of H_2 $v = 1 \rightarrow 0$ S(1) and NH_3(3, 3), respectively, the latter scaled by 10^{-16}. The range of our H_2 observation is denoted by two vertical lines.

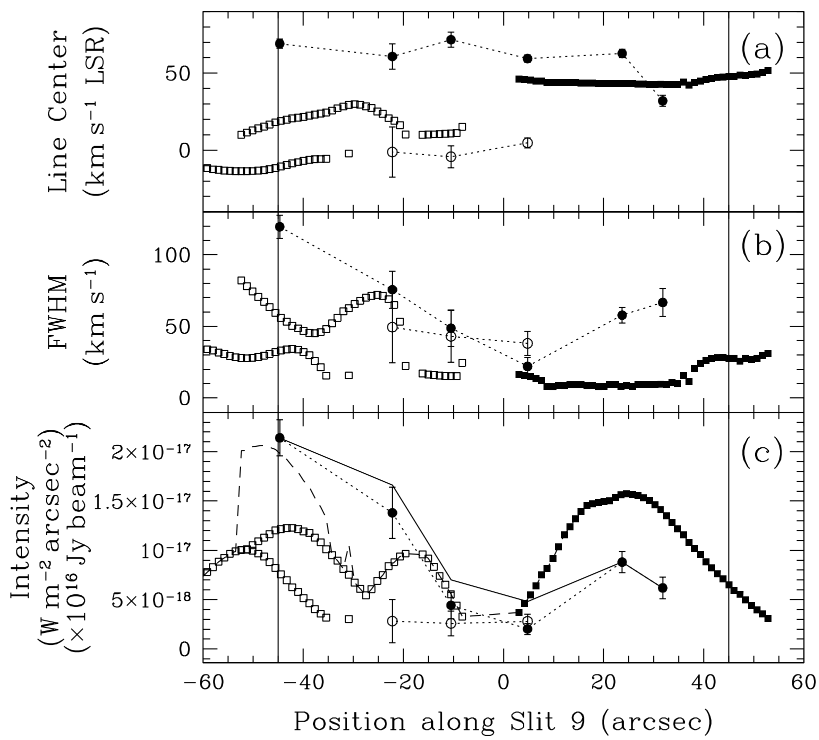

Figure 5. Derived line parameters for the spectra along slit 9. Indicated positions are as in Fig. 3; positive towards the north-east. Identities of plotted quantities are as in Fig. 4. The decrease in NH_3 flux at positions greater than +30 arcsec is a result of reduced sensitivity at the edge of the mosaic (McGary et al. 2001).

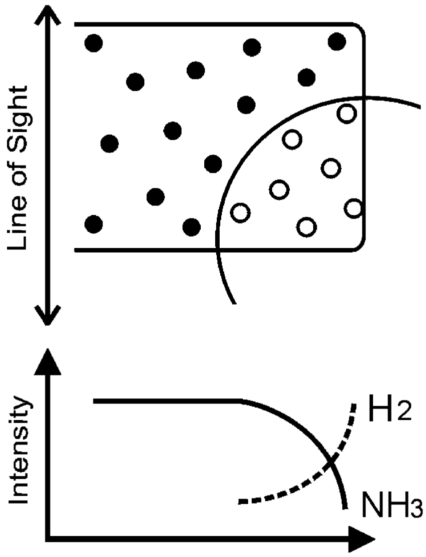

Figure 6. Schematic diagram of Sgr A East and the GMC M−0.02 − 0.07 along the line of sight. The large partial circle shows the boundary of Sgr A East and the small circles enveloped in a square (M−0.02 − 0.07) represent the clumpy structure of the cloud (see Section 3.3). Open circles are clumps that are being penetrated by shocks, which have destroyed NH_3 but have excited the H_2 into emission. The resulting intensity distribution shows a similar trend to the observed results [see the +50 km s^{-1} components in Figs 4(c) and 5(c)].

On the other hand, the fact that the two H_2 velocity components overlap along the line of sight, yet are roughly equally bright, seems somewhat unlikely, as one must be attenuated by the molecular cloud associated with the other. The rough equality might be explained by clumpiness of the foreground cloud, regardless of which one is in the foreground, where a small filling factor of high-density clumps are embedded within a less dense medium (Burton, Hollenbach & Tielens 1990). The size of such clumps seems to be 10^{-4}–10^{-3} pc (Garay, Moran & Reid 1987; Churchwell et al. 1987), which is smaller than our resolution of ∼1 arcsec (∼4 × 10^{-2} pc at the distance of ∼8.5 kpc to the Galactic Centre). As illustrated in Fig. 6, this clumpy structure could explain both the observed decrease of NH_3 line emission and the observed increase of H_2 line emission toward the edge of the cloud [see the +50 km s^{-1} components in Figs 4(c) and 5(c)].

4 CONCLUSION

We observed the north-eastern part of the Sgr A East shell in order to investigate its interaction with the GMC M−0.02 − 0.07. The bright H_2 $v = 1 \rightarrow 0$ S(1) emission is strong evidence that Sgr A East is physically adjacent to, and interacting with, M−0.02 − 0.07.

By comparing the relative intensities of H_2 $v = 1 \rightarrow 0$ S(1) and H_2 $v = 2 \rightarrow 1$ S(1) emission, the distribution of the H_2 $v = 2 \rightarrow 1$ S(1)/$v = 1 \rightarrow 0$ S(1) line ratio, and the radial velocities of the H_2 emission, we can to some extent distinguish between excitation mechanisms for the H_2. The line ratios tend to support emission in either fast J-type shocks or a dense PDR. However, on considering the bright H_2 $v = 1 \rightarrow 0$ S(1) intensity, the large linewidths and the spatial variation in the line ratio, we conclude that a combination of C-type shocks and fluorescence is required. The presence of shocks is direct evidence that Sgr A East is driving into the surrounding material, and is consistent with the detection of 1720-MHz OH masers to the north of the CND and to the south of Sgr A East (Yusef-Zadeh et al. 1996). Very recently Karlsson et al. (2003) detected the 1720-MHz OH masers also at two positions near our target region, which is more direct evidence supporting our conclusion on the C-type shocks.

The H_2 emission covers most parts of our targeted region (90 × 27 arcsec^2). The line profiles are made up of two velocity components, both of which extend over a significant portion of the region (15 × 27 arcsec^2). We find that the NH_3(3, 3) emission lines observed by McGary et al. (2001) also show a similar kinematic structure, with almost the same velocities. We suggest that the H_2 line emission arises at the interfaces between Sgr A East and two independent molecular clouds, with line-of-sight velocities of ∼+50 km s^{-1} (M−0.02 − 0.07) and ∼0 km s^{-1} (the northern ridge). Both the observed two velocity components of the H_2 emission and the difference in the intensity distributions between the H_2 and NH_3 emission can be understood if the molecular clouds are composed of small dense clumps with a very small filling factor.

To study the origin and evolution of Sgr A East, it would be important to know the total H_2 luminosity and the total cooling rate (based on that) over the interaction region, which could be compared with those of well-studied supernova remnants. However, it is very difficult to estimate them with the small amount of information that we have at present. Given the uncertainty in the emission mechanisms, even estimating the total H_2 luminosity in the small mapped region would be difficult, without considering the entire interaction region. It would be premature for us to estimate the required energy to make the Sgr A East shell. We will be able to do this in the future, after observations of more of the interaction region.

ACKNOWLEDGMENTS

We give special thanks to Young-Sam Yu and Tae-Hyun Kim for their help with the observation. Fig. 1 has been reproduced, with permission, from Astrophysical Journal, published by The University of Chicago Press. (©2001 by the American Astronomical Society. All rights reserved.) The United Kingdom Infrared Telescope is operated by the Joint Astronomy Centre on behalf of the UK Particle Physics and Astronomy Research Council. This work was financially supported by the BK21 Project of the Korean Government. TRG's research is supported by the Gemini Observatory, which is operated by the Association of Universities for Research in Astronomy, Inc., on behalf of the international Gemini partnership of Argentina, Australia, Brazil, Canada, Chile, the United Kingdom and the United States of America.

REFERENCES

Black J. H., van Dishoeck E. F., 1987, ApJ, 322, 412
Burton M. G., 1992, Aust. J. Phys., 45, 463
Burton M. G., Hollenbach D. J., Tielens A. G. G. M., 1990, ApJ, 365, 620
Catchpole R. M., Whitelock P. A., Glass I. S., 1990, MNRAS, 247, 479
Churchwell E., Wood D. O. S., Felli M., Massi M., 1987, ApJ, 321, 516
Coil A. L., Ho P. T. P., 2000, ApJ, 533, 245
Davis C. J., Smith M. D., 1995, ApJ, 443, L41
Draine B. T., McKee C. F., 1993, ARA&A, 31, 373
Fatuzzo M., Melia F., Yusef-Zadeh F., Markoff S., 1999, in Falcke H., Cotera A., Duschl W. J., Melia F., Rieke M. J., eds, ASP Conf. Ser. Vol. 186, The Central Parsecs of the Galaxy. Astron. Soc. Pac., San Francisco, p. 560
Fernandes A. J. L., Brand P. W. J. L., Burton M. G., 1997, MNRAS, 290, 216
Frail D. A., Goss W. M., Reynoso E. M., Green A. J., Otrupcek R., 1996, AJ, 111, 1651

Garay G., Moran J. M., Reid M. J., 1987, ApJ, 314, 535
Gatley I., Jones T. J., Hyland A. R., Beattie D. H., Lee T. J., 1984, MNRAS, 210, 565
Genzel R., Stacey G. J., Harris A. I., Geis N., Graf U. U., Poglitsch A., Sutzki J., 1990, ApJ, 356, 160
Goss W. M., Schwarz U. J., Ekers R. D., van Gorkom J. H., 1983, in Danziger J., Gorenstein P., eds, Proc. IAU Symp. 101, Supernova Remnants and Their X-Ray Emission. Reidel, Dordrecht, p. 65
Ho P. T. P., Ho L. C., Szczepanski J. C., Jackson J. M., Armstrong J. T., Barrett A. H., 1991, Nat, 350, 309
Hollenbach D., McKee C. F., 1989, ApJ, 342, 306
Jones T. W., 1974, A&A, 30, 37
Karlsson R., Sjouwerman L. O., Sandqvist Aa., Whiteoak J. B., 2003, A&A, submitted
Kaufman M. J., Neufeld D. A., 1996, ApJ, 456, 611
Khokhlov A., Melia F., 1996, ApJ, 457, L61
Kwan J., 1977, ApJ, 216, 713
McGary R. S., Coil A. L., Ho P. T. P., 2001, ApJ, 559, 326
Maeda Y. et al., 2002, ApJ, 570, 671
Mezger P. G., Zylka R., Salter C. J., Wink J. E., Chini R., Kreysa E., Tuffs R., 1989, A&A, 209, 337
Mezger P. G., Duschl W. J., Zylka R., 1996, ARA&A, 7, 289
Mountain C. M., Robertson D. J., Lee T. J., Wade R., 1990, in Crawford D. L., ed., Proc. SPIE Vol. 1235, Instrumentation in Astronomy VII. SPIE, Bellingham, p. 25
Novak G., 1999, in Falcke H., Cotera A., Duschl W. J., Melia F., Rieke M. J., eds, ASP Conf. Ser. Vol. 186, The Central Parsecs of the Galaxy. Astron. Soc. Pac., San Francisco, p. 488
Pak S., Jaffe D. T., Keller L. D., 1996a, ApJ, 457, L43
Pak S., Jaffe D. T., Keller L. D., 1996b, in Gredel R., ed., ASP Conf. Ser. Vol. 102, The Galactic Center. Astron. Soc. Pac., San Francisco, p. 28
Pak S., Jaffe D. T., van Dishoeck E. F., Johansson L. E. B., Booth R. S., 1998, ApJ, 498, 735
Richter M. J., Graham J. R., Wright G. S., 1995, ApJ, 454, 277
Serabyn E., Lacy J. H., Achtermann J. M., 1992, ApJ, 395, 166
Smith M. D., 1995, A&A, 296, 789
Sternberg A., Dalgarno A., 1989, ApJ, 338, 197
Takami M., Usuda T., Sugai H., Kawabata H., Suto H., Tanaka M., 2000, ApJ, 529, 268
Usuda T., Sugai H., Kawabata H., Inoue M. Y., Kataza H., Tanaka M., 1996, ApJ, 464, 818
Wardle M., Yusef-Zadeh F., Geballe T. R., 1999, in Falcke H., Cotera A., Duschl W. J., Melia F., Rieke M. J., eds, ASP Conf. Ser. Vol. 186, The Central Parsecs of the Galaxy. Astron. Soc. Pac., San Francisco, p. 432
Woosley S. E., Eastman R. G., Schmidt B. P., 1999, ApJ, 516, 788
Yusef-Zadeh F., Morris M., 1987, ApJ, 320, 545
Yusef-Zadeh F., Roberts D. A., Goss W. M., Frail D. A., Green A. J., 1996, ApJ, 466, L25
Yusef-Zadeh F., Roberts D. A., Goss W. M., Frail D. A., Green A. J., 1999a, ApJ, 512, 230
Yusef-Zadeh F., Stolovy S. R., Burton M., Wardle M., Melia F., Lazio T. J. W., Kassim N. E., Roberts D. A., 1999b, in Falcke H., Cotera A., Duschl W. J., Melia F., Rieke M. J., eds, ASP Conf. Ser. Vol. 186, The Central Parsecs of the Galaxy. Astron. Soc. Pac., San Francisco, p. 197
Yusef-Zadeh F., Stolovy S. R., Burton M., Wardle M., Ashley M. C. B., 2001, ApJ, 560, 749

This paper has been typeset from a TEX/LATEX file prepared by the author.